Universal Viscosity Behavior of Polymer Nanocomposites

Jagannathan T. Kalathi, Gary S. Grest, and Sanat K. Kumar

Phys. Rev. Lett. **109**, 198301 — Published 7 November 2012

DOI: 10.1103/PhysRevLett.109.198301

Universal Viscosity Behavior of Polymer Nanocomposites

Jagannathan T. Kalathi,[1] Gary S. Grest,[2] and Sanat K. Kumar[1,*]

[1]Department of Chemical Engineering, Columbia University, New York, NY 10027, USA
[2]Sandia National Laboratories, Albuquerque, New Mexico 87185, USA
(Dated: Aug 14, 2012)

Abstract

Non-equilibrium molecular dynamics simulations are used to show that the shear viscosity of a polymer melt can be significantly reduced when filled with small energetically neutral nanoparticles, apparently independent of the polymer's chain length. Analogous to solvent molecules, small nanoparticles act akin to plasticizers and reduce the viscosity of a polymer melt. This effect, which persists for particles whose sizes are as large as the chain size or the entanglement mesh size, whichever is smaller, can be overcome by making the chain-nanoparticle interactions significantly attractive. Our simulations allow us to systematically organize the viscosity data of filled polymer melts, and thus provide a strong basis from which to predict the flow behavior of these commercially important class of materials.

Micron-sized spherical fillers increase the viscosity of a pure polymer melt from η_p to a value, η, predicted by the Einstein-Batchelor law: $\frac{\eta}{\eta_p} = 1 + 2.5\phi + 6.2\phi^2$ .. where ϕ is the particle volume fraction.[1-3] However, for nanosized fillers, η can be reduced or increased relative to the pure polymer.[4-12] While there have been extensive simulations of nanocomposites,[13-18] most have focused on the importance of polymer-NP interactions on flow behavior.[9, 19] The complicated, and poorly understood, dependence of η on NP size, chain size, and polymer-NP interactions, are the issues we study here.

Here polymer chains are represented by the Kremer-Grest model.[20] Non-bonded monomers interact through the Lenard-Jones (LJ) potential truncated at $r_c = 2.5\sigma$; σ is the monomer size and ε is the energy scale. Adjacent chain monomers are bonded by a FENE potential.[20] A bond-bending potential, $V(\theta) = k_\theta[1 + cos\theta]$, with $k_\theta = 0.75\varepsilon$ is used to reduce the entanglement chain length N_e from 85 to 45.[21] We consider four different melts with chains of length N=40, 100, 200 and 400, respectively, i.e., from unentangled to entangled. Two NP models are employed. In the "rough" NP model, a collection of LJ atoms, each equivalent to a chain monomer, are held together in an FCC lattice. The polymer-NP interaction is the LJ potential with a well depth ε_{np}, which is either ε (athermal) or 2ε (attractive) ($r_c = \frac{\sigma_{NP}}{2} + \sigma$ for $\sigma_{NP} \geq 3$; $r_c = 2.5\sigma$ otherwise). The interaction strength between two NP beads is $\varepsilon_{nn} = \varepsilon$ with $r_c = \sigma$. (i.e., repulsive). The interactions between a pair of "smooth" spherical NPs of diameter σ_{NP} is determined by integrating over all the LJ atoms in the two NPs.[22-25] The NP mass is equal to its volume multiplied by a number density, $\rho\sigma^3$=1.0. The well depth of the effective NP-NP pair potential is thus governed by a Hamaker prefactor, A_{nn}.[25] From here $A_{nn} \equiv 4\pi^2\varepsilon = 39.48\varepsilon$. We used $r_c = \sigma_{NP}$ so that NP-NP interactions are purely repulsive. While a corresponding analysis for NP-polymer interactions would lead to $A_{np} = 24\pi\varepsilon \approx 72\varepsilon$, this

A_{np} yields immiscible composites. A larger $A_{np} = 100\varepsilon$ has to be used to represent "athermal" NP-polymer interactions and $A_{np} = 400\varepsilon$ is used for favorable attractions ($r_c = \frac{\sigma_{NP}}{2} + 4\sigma$). The NP's are spatially well dispersed under all conditions studied. We simulated 500 chains for the neat melts. Filled systems consisted of 500-1033 chains for N=400 and 500-2000 chains for N=40, 100 and 200. The NP loading $\phi_{NP} = \frac{\sigma_{NP}^3 N_{NP}}{(\sigma_{NP}^3 N_{NP} + \sigma^3 N N_P)}$ is set to its desired value by varying N_{NP} and N_P, the number of NP and chains, respectively.

Systems of chain length N=100, 200 and 400, respectively, are equilibrated following the double-bridging procedure with $T^* = \frac{k_B T}{\epsilon} = 1$, and pressure $P^* = 0$.[26] The N=40 melt is equilibrated by running isobarically at $P^* = 0$, and then at constant volume till the chains move their own size. We integrate the SLLOD (which adopts the transpose of the **qp**-DOLLS tensor) equations of motion[27] at a strain rate, $\dot{\gamma}$, with the Large-scale Atomic/Molecular Massively Parallel Simulator (LAMMPS) code,[28] using a time step of δt=0.005 or 0.01 τ, where $\tau = \sqrt{m\sigma^2/\varepsilon}$. The pressure tensor, which is stored over runs 10 $\dot{\gamma}^{-1}$ in length,[29] is found to have diagonal components equal to zero with an accuracy better than 10^{-2}. The shear viscosity is calculated using $\eta = -\frac{\langle P_{xz} \rangle}{\dot{\gamma}}$, where $\langle P_{xz} \rangle$ is the *xz*-component of the pressure tensor along the flow and gradient directions, respectively. At high $\dot{\gamma}$, the time-dependent viscosity reaches a plateau when $\dot{\gamma} t > 1$, after an initial overshoot. This plateau is used to estimate η. For low $\dot{\gamma}$ there is no such overshoot.

All four neat melts exhibit shear thinning (Fig. 1). The N=100 and 200 data reach their Newtonian plateaus for $\dot{\gamma}^* \approx 10^{-5}$ and 10^{-6}, respectively, while the N=400 melt does not plateau even for $\dot{\gamma}^* = 10^{-7}$. For $\dot{\gamma}^* = 10^{-7}$, we need 75 days on 216 processing cores on the Cray XE6 Hopper at NERSC to get an estimate of η. Runs for lower $\dot{\gamma}^*$ are thus infeasible, and so the results for N=400 may not be in the Newtonian regime. Figure 1

also presents results for two different sized rough NPs at $\phi_{NP} = 0.11$. For these athermal polymer-NP mixtures,[4, 5] the insets show that the ratio of viscosity of the filled system to the neat melt is essentially independent of $\dot{\gamma}^*$, especially for large σ_{NP}, and changes by ~20% even for the smallest particle size. Thus, even though we do not access $\dot{\gamma} \to 0$ for N= 400, we can still draw meaningful conclusions on the NP's effect on η.

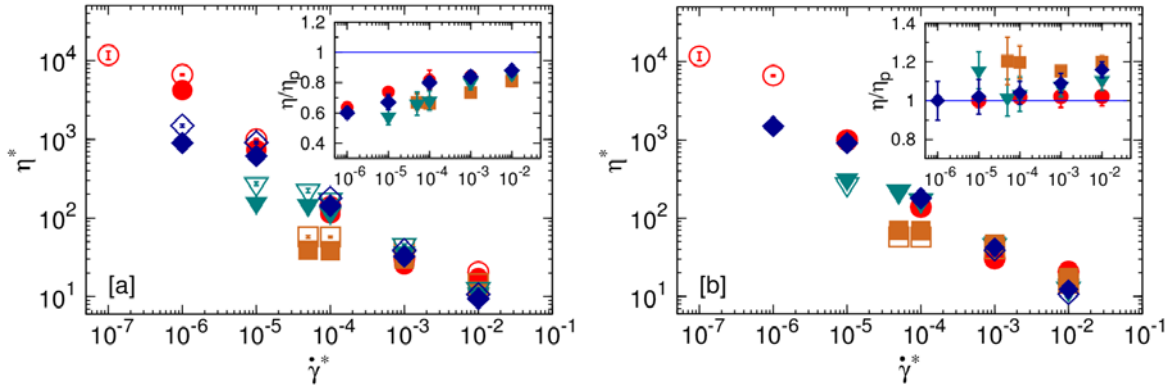

Figure 1: Reduced shear viscosity, $\eta^* = \frac{\eta\sigma^3}{\varepsilon\tau}$ *vs.* reduced strain rate $\dot{\gamma}^* = \dot{\gamma}\tau$. Neat and NP-filled melts are represented by open and closed symbols, respectively, at a fixed $\phi_{NP} = 0.11$ for N=40 (■), N=100 (▼), N=200 (◆), and N=400 (●). (a) $\sigma_{NP} = 1\sigma$ (b) $\sigma_{NP} = 10\sigma$. Inset shows the ratio of the filled to neat melt viscosity as a function of $\dot{\gamma}^*$.

Figures 2(a) and (b) show the effect of σ_{NP} on η at $\phi_{NP} = 0.11$ for N=40 and 400, respectively. We see that a rough NP with $\varepsilon_{np} = \varepsilon$ behaves akin to a smooth NP with A_{np}=100ε - this A_{np} therefore corresponds to an athermal nanocomposite, and particle smoothness does not alter the conclusions drawn. For N=40 [Fig. 2(a)] and neutral rough NPs the η is lower than that of the pure melt, η_p, for $\sigma_{NP} \leq 5\sigma$. The results for the longer chains are qualitatively consistent, except that the crossover to viscosity ratios greater than 1 occurs for progressively larger σ_{NP} [Fig. 2(b)]. Predictably, the viscosity becomes larger than the athermal case if the NP-polymer interactions are favorable ($\varepsilon_{np} = 2\varepsilon$) [Figs. 2(a) & (b)]. For N=40 the viscosity is larger than the neat melt for all σ_{NP}, while for N=400 we get η reductions for small enough particles. Next, we consider the role of ϕ_{NP} on η for neutral NPs. The N=40 shows a monotonic increase for $\sigma_{NP} =$

10σ, consistent with the Batchelor law (Fig. 2c). In contrast, for $\sigma_{NP} = \sigma$, the viscosity decreases with increasing ϕ_{NP} (Fig. 2c). Similarly, the N=100 melt shows a monotonic increase for $\sigma_{NP} = 10\sigma$ (Fig. 2d). For $\sigma_{NP} = 8\sigma$ in N=100 and $\sigma_{NP} = 10\sigma$ in N=400, the η initially drops with increasing ϕ_{NP}, and then it increases beyond the pure melt value for large enough NP loading, as observed experimentally.[6]

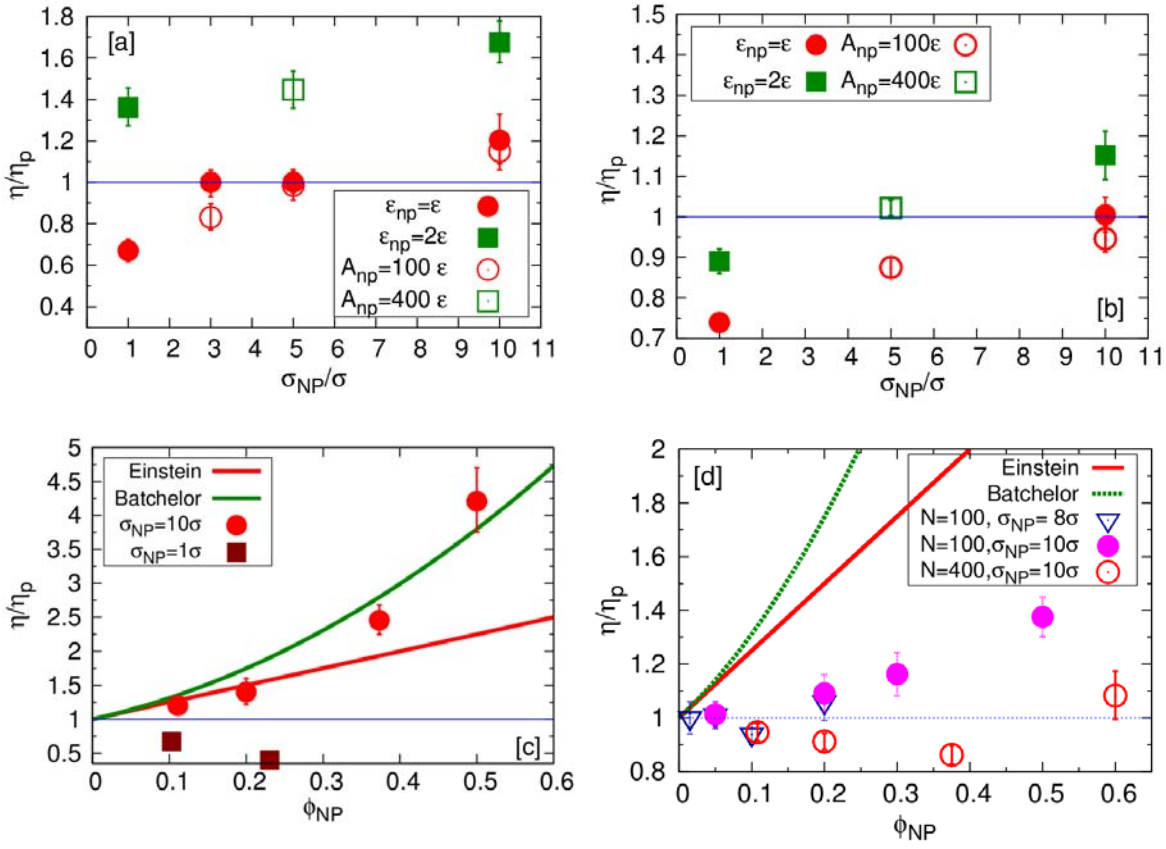

Figure 2: Effect of NP size and type of interaction between the NP and polymer on shear viscosity for (a) N=40, $\dot{\gamma}^* \to 0$; (b) N=400, $\dot{\gamma}^* = 10^{-5}$ for ϕ_{NP}= 0.11. Dependence of viscosity on loading of neutral NP for (c) N=40 with (σ_{NP} = 10σ and 1σ) as $\dot{\gamma}^* \to 0$; (d) N=100 with (σ_{NP} = 8 and 10σ) as $\dot{\gamma}^* \to 0$ and N=400 with (σ_{NP} = 10σ) at $\dot{\gamma}^* = 10^{-5}$. In all the plots the closed symbols correspond to rough NP, while the open symbols to smooth NP. In (c) and (d), we show the Einstein and Batchelor predictions.

We now examine the molecular origins of these results. Adding NP to a melt can either change the local friction or N_e. Riggleman et al.[30] showed that "athermal" NPs reduce N_e from 62.3 (pure melt) to 56.4 (N=500, $\sigma_{NP} = 5\sigma$, ϕ_{NP}=0.15). In contrast,

completely repulsive mixtures of NPs and polymers (N=500, $\sigma_{NP} = 10\sigma$) show that N_e increases with NP loading.[31] Before discussing our primitive path analysis (PPA) results, we touch on a philosophical point. In the limit of large particles ($\sigma_{NP} \geq 5\sigma$), it makes sense to fix the particles, which are much less mobile than the chains, in the PPA. (Note that we found little difference by fixing the particles or not in this limit.) In contrast, allowing smaller NPs to move or not makes a qualitative difference. We estimate N_e for the N=400 melt with smooth NP at ϕ_{NP}= 0.11 by allowing the NP to move.[32]

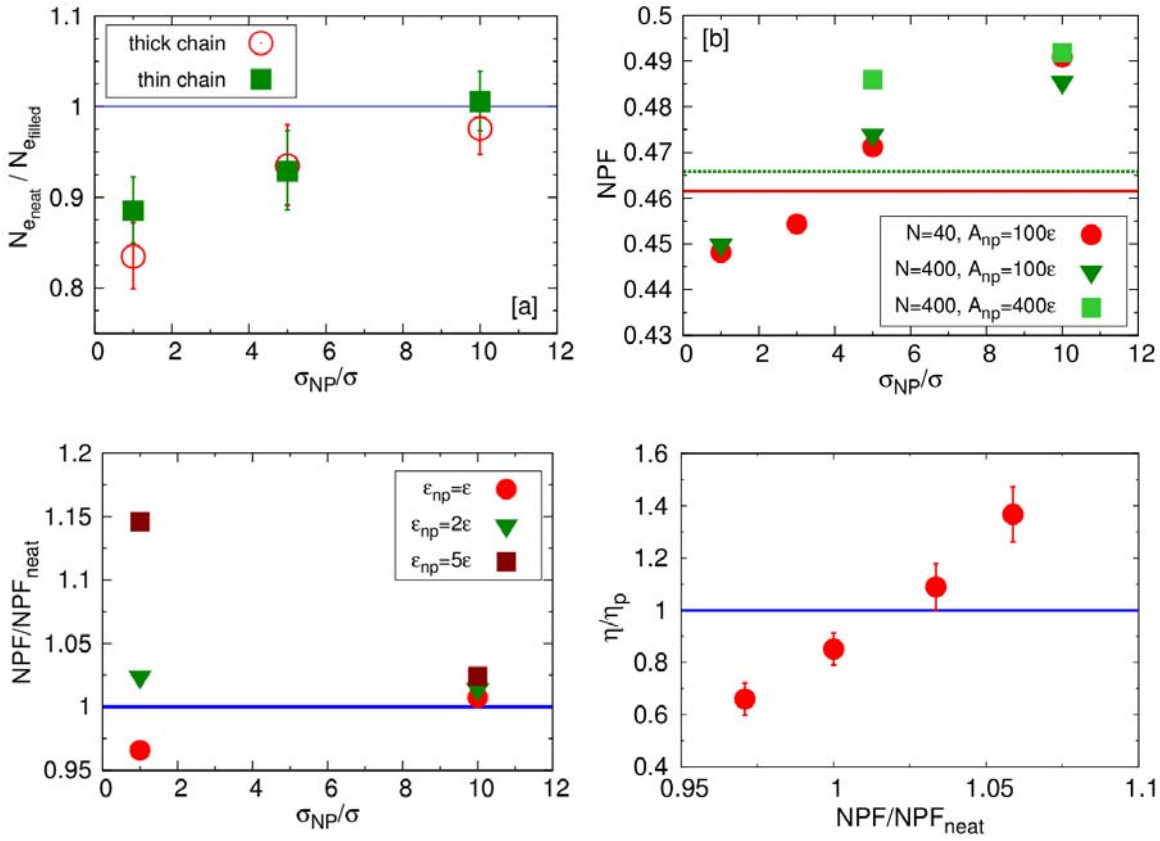

Figure 3: (a) Effect of σ_{NP} on N_e for N=400 melts filled with smooth NPs with A_{np}=100ε and $\phi_{NP} = 0.11$. (b) Net packing fraction, NPF, as a function of smooth NP size for $\phi_{NP} = 0.11$. The lines represent the pure melts; (c) Effect of NP-polymer bead interaction strength on NPF for N=400 melts and rough NPs. $\phi_{NP} = 0.11$. Line represents the pure melt. (d) Dependence of η on NPF for the N=40 melt with neutral $\sigma_{NP} = 1\sigma$ NPs. Line is the pure melt.

Figure 3a plots (N/N_e), normalized by its pure melt value. The N_e increases significantly when particle size decreases (Fig. 3a), implying that these small NPs act

akin to plasticizers. The N_e recovers to its bulk value for $\sigma_{NP} = 10\sigma$, a result that should be contrasted to the work of Li et al.[31] on repulsive systems, who found a decrease in entanglement for the same NP size. Tuteja et al.[5] found that N_e is unaffected by NP for σ_{NP} ≥5 nm. On assuming a Kuhn length of 1nm, we also find that N_e practically equals its bulk value for these σ_{NP}.[5] We conclude that our results, which include athermal attractions between the NP and the chains, are perhaps more relevant experimentally than calculations that treat these systems through purely repulsive interactions.

Next we consider free volume effects.[4, 5] At $P^* = 0$ the density must change on adding NPs to the polymer. Fig. 3(b) quantifies this idea by plotting the net packing fraction, $NPF = \frac{\pi\left(N_{NP}\sigma_{NP}^3 + N_P\sigma^3\right)}{6V}$, where V is the simulation volume, as a function of σ_{NP} at $\phi_{NP} = 0.11$. As anticipated, adding athermal small NPs causes a strong drop in the NPF, with this result being reversed by NP-polymer attractions [Fig. 3(c)] or by increasing σ_{NP}.

In addition to equation-of-state effects, Ganesan et al.[17] suggested that hydrodynamic effects and wall slip could alter the monomer friction coefficient. To understand the relative importance of flow *vs.* free volume effects, we examined the filled N=40 melt's viscosity as a function of NPF [Fig. 3(d)]. Obviously, the pressure changes in these calculations. At a NPF ≈ 0.45, which corresponds to P^*=0 for the filled system, the η^* ≈38. For the filled melt at NPF=0.46, which is the neat melt density, we find η^* ≈50. Since η^* ≈57 for the pure melt at P^*=0, it follows that ≈2/3 of the viscosity drop on the addition of NP to an unentangled melt is due to equation-of-state effects, with 1/3 to other flow factors. We conclude that for small particles the changes in η have contributions from entanglements, flow and equation-of-state effects. In contrast, changes in entanglement effects appear to play a minor role for large particles.

We now place our results in the context of the unexplained experimental trends for the viscosity of filled polymers.[4-12] Fig. 4a plots simulation data for $\varepsilon_{np} = \varepsilon$, which are

germane to the experiments where the NP and the melts have the same chemical structure,[4, 5] while chemically dissimilar mixtures are considered in Fig. 4b.[6-12]

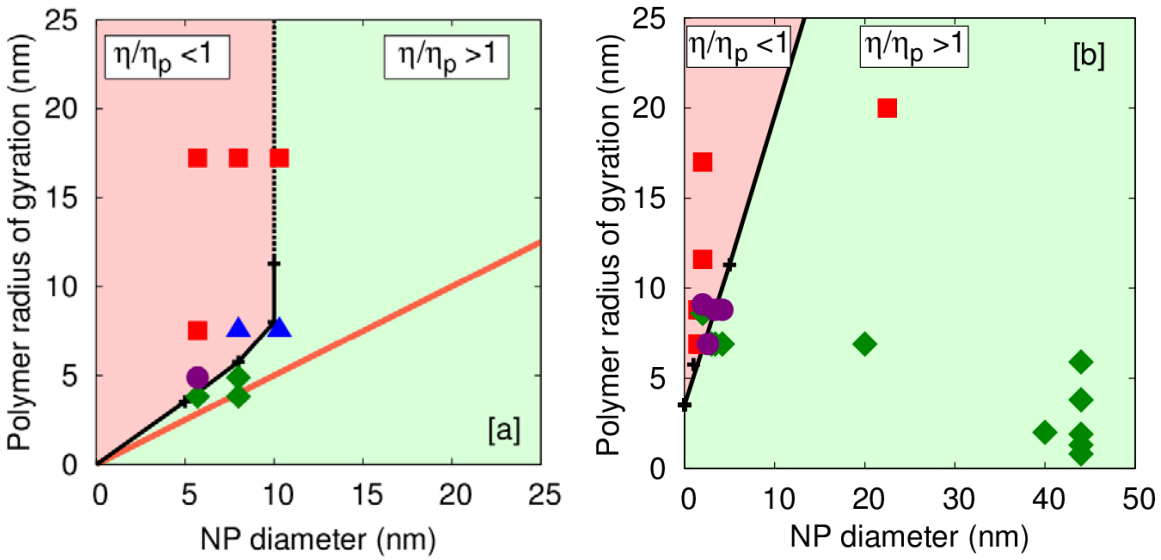

Figure 4: Polymer radius of gyration *vs.* NP diameter. The experimental data correspond to (■) $\eta/\eta_p < 1$, (◆) $\eta/\eta_p > 1$, (●) $\eta/\eta_p \approx 1$ at low NP loading and (▲) is where η shows an initial increase of viscosity with NP loading followed by a decrease. (a) Experimental data for athermal systems is from [4, 5]. Systems above the orange line should be miscible. The black "viscosity" line is extrapolated from our simulations. (b) Corresponding plot for "thermal" NP/polymer systems. Only the viscosity line is shown. Data are from [6-12].

In Fig. 4a the "solubility" line from [33] suggests that the experiments correspond to miscible NP-polymer mixtures. The "viscosity" line, from our simulations, separates regions where the nancomposite's η is smaller than *vs.* larger than the pure melt. (A Kuhn length of 1nm was used to compare the simulations to experiments.) The slope of the viscosity line is quite different for short *vs.* long chains. For short chains, the viscosity crossover occurs when the NP size is comparable to R_g. In contrast, our limited data for large R_g suggest that the line is nearly vertical. Apparently, the RMS end-to-end distance for an entanglement strand ($= \sqrt{2.2 \times 45} \approx 10\sigma$), a proxy for the entanglement mesh size defines the crossover.[2-6, 17] (The entanglement molecular weight of PS ~14 kDa[34] leads to R_e~ 8.2 nm, which is comparable to the simulation estimates.) This "viscosity" line satisfactorily explains most of the experimental trends for the athermal nanocomposites.

The only exceptions are the two blue triangles where the viscosity initially increases on adding NPs, but then decreases. Fig. 4b for polymers filled with inorganic NPs,[6-12] emphasizes the critical role of NP-polymer miscibility – the experimental data on the bottom right of Fig. 4(b) would be immiscible if the systems were athermal. While we expect system-to-system variations, Hooper and Schweizer suggest that miscibility is only attained over a narrow range of NP-chain attractions.[35] We therefore characterize all miscible blends through the ansatz that $\epsilon_{np} = 2\epsilon$. Empirical justification for this sweeping assumption comes from the fact that the viscosity line derived in this manner serves to reliably separate experimental systems with increased *vs.* reduced viscosity relative to the melt, with one exception (Fig. 4b).[7] Since Figs. 4 organize a relatively comprehensive set of available experimental data, we believe that it embodies a first cut at a "universal" behavior for this class of problems, and provides us with a quantitative basis to understand the flow behavior of these systems.

Financial support from the National Science Foundation (DMR-1006514) and the National Institute for Nano Engineering at Sandia is gratefully acknowledged. This research used resources obtained through the Advanced Scientific Computing Research (ASCR) Leadership Computing Challenge (ALCC) at the National Energy Research Scientific Computing Center (NERSC), which is supported by the Office of Science of the United States Department of Energy under Contract No. DE-AC02-05CH11231. Sandia National Laboratories is a multi-program laboratory managed and operated by Sandia Corporation, a wholly owned subsidiary of Lockheed Martin Corporation, for the U.S. Department of Energy's National Nuclear Security Administration under contract DE-AC04-94AL85000. We thank Kurt Kremer, Ralph Colby, and especially Venkat Ganesan and Ken Schweizer for very useful suggestions on this work.

References

1 T. Kataoka, T. Kitano, M. Sasahara, and K. Nishijima, Rheologica Acta **17**, 149 (1978).
2 U. Yamamoto and K. S. Schweizer, J. Chem. Phys. **135** (2011).
3 L. H. Cai, S. Panyukov, and M. Rubinstein, Macromolecules **44**, 7853 (2011).
4 M. E. Mackay, T. T. Dao, A. Tuteja, D. L. Ho, B. Van Horn, H. C. Kim, and C. J. Hawker, Nature Materials **2**, 762 (2003).
5 A. Tuteja, M. E. Mackay, C. J. Hawker, and B. Van Horn, Macromolecules **38**, 8000 (2005).
6 K. Nusser, G. J. Schneider, W. Pyckhout-Hintzen, and D. Richter, Macromolecules **44**, 7820 (2011).
7 S. Jain, J. G. P. Goossens, G. W. M. Peters, M. van Duin, and P. J. Lemstra, Soft Matter **4**, 1848 (2008).
8 G. V. Gordon, R. G. Schmidt, M. Quintero, N. J. Benton, T. Cosgrove, V. J. Krukonis, K. Williams, and P. M. Wetmore, Macromolecules **43**, 10132 (2010).
9 S. Y. Kim and C. F. Zukoski, Soft Matter **8**, 1801 (2012).
10 R. S. Ndong and W. B. Russel, Journal of Rheology **56**, 27 (2012).
11 B. J. Anderson and C. F. Zukoski, Macromolecules **42**, 8370 (2009).
12 R. G. Schmidt, G. V. Gordon, C. A. Dreiss, T. Cosgrove, V. J. Krukonis, K. Williams, and P. M. Wetmore, Macromolecules **43**, 10143 (2010).
13 G. D. Smith, D. Bedrov, L. W. Li, and O. Byutner, J Chem Phys **117**, 9478 (2002).
14 F. W. Starr, J. F. Douglas, and S. C. Glotzer, J Chem Phys **119**, 1777 (2003).
15 M. Vladkov and J. L. Barrat, Macromolecular Theory and Simulations **15**, 252 (2006).
16 S. Sen, J. D. Thomin, S. K. Kumar, and P. Keblinski, Macromolecules **40**, 4059 (2007).
17 V. Ganesan, V. Pryamitsyn, M. Surve, and B. Narayanan, J. Chem. Phys. **124** (2006).
18 M. Wang and R. J. Hill, Soft Matter **5**, 3940 (2009).
19 B. J. Anderson and C. F. Zukoski, Langmuir **26**, 8709 (2010).
20 K. Kremer, G. S. Grest, and I. Carmesin, Phys Rev Lett **61**, 566 (1988).
21 R. S. Hoy, K. Foteinopoulou, and M. Kroger, Physical Review E **80** (2009).
22 R. Everaers and M. R. Ejtehadi, Physical Review E **67** (2003).
23 G. S. Grest, Q. F. Wang, P. in't Veld, and D. J. Keffer, J. Chem. Phys. **134** (2011).
24 P. J. in' t Veld, M. A. Horsch, J. B. Lechman, and G. S. Grest, J. Chem. Phys. **129** (2008).
25 P. J. in't Veld, S. J. Plimpton, and G. S. Grest, Comput Phys Commun **179**, 320 (2008).
26 R. Auhl, R. Everaers, G. S. Grest, K. Kremer, and S. J. Plimpton, J. Chem. Phys. **119**, 12718 (2003).
27 M. E. Tuckerman, C. J. Mundy, S. Balasubramanian, and M. L. Klein, J Chem Phys **106**, 5615 (1997).
28 S. Plimpton, J. Comput. Phys. **117**, 1 (1995).
29 W. B. Lee and K. Kremer, Macromolecules **42**, 6270 (2009).
30 R. A. Riggleman, G. Toepperwein, G. J. Papakonstantopoulos, J. L. Barrat, and J. J. de Pablo, J. Chem. Phys. **130** (2009).
31 Y. Li, M. Kroger, and W. K. Liu, Physical Review Letters **109**, 118001 (2012).

[32] R. Everaers, S. K. Sukumaran, G. S. Grest, C. Svaneborg, A. Sivasubramanian, and K. Kremer, Science **303**, 823 (2004).
[33] M. E. Mackay, A. Tuteja, P. M. Duxbury, C. J. Hawker, B. Van Horn, Z. B. Guan, G. H. Chen, and R. S. Krishnan, Science **311**, 1740 (2006).
[34] L. J. Fetters, D. J. Lohse, D. Richter, T. A. Witten, and A. Zirkel, Macromolecules **27**, 4639 (1994).
[35] J. B. Hooper and K. S. Schweizer, Macromolecules **39**, 5133 (2006).